CONDENSED MATTER PHYSICS

Magnetizing topological surface states of Bi_2Se_3 with a CrI_3 monolayer

Yusheng Hou[1], Jeongwoo Kim[1,2], Ruqian Wu[1]*

To magnetize surfaces of topological insulators without damaging their topological feature is a crucial step for the realization of the quantum anomalous Hall effect (QAHE) and remains as a challenging task. Through density functional calculations, we found that adsorption of a semiconducting two-dimensional van der Waals (2D-vdW) ferromagnetic CrI_3 monolayer can create a sizable spin splitting at the Dirac point of the topological surface states of Bi_2Se_3 films. Furthermore, general rules that connect different quantum and topological parameters are established through model analyses. This work provides a useful guideline for the realization of QAHE at high temperatures in heterostructures of 2D-vdW magnetic monolayers and topological insulators.

INTRODUCTION

Topological insulators (TIs) are emergent quantum materials that have nontrivial bandgaps in their bulks along with topologically protected surface or edge states at boundaries (*1*). For the design of the next-generation spintronic devices (*2*, *3*), especially those based on the quantum anomalous Hall effect (QAHE), it is crucial to find efficient ways to magnetize their topological surface states (TSSs) while maintaining their topological features (*4*–*6*). The conventional approach is doping magnetic ions into TIs (*7*–*11*), and the QAHE has been successfully realized in Cr- or V-doped $(Bi, Sb)_2Te_3$ thin films (*9*–*11*). However, it is still very challenging to control the distribution and magnetic order of dopants in TIs, and the critical temperature (T_c) for the observation of QAHE is extremely low (30 mK) (*9*). A promising alternative way to magnetize TSSs is through the interfacial magnetic proximity effect by putting three-dimensional (3D) magnetic insulators on TIs (*12*–*18*). Unfortunately, the interfacial hybridization in most of these heterostructures is too strong, and TSSs are either damaged or shifted away from the Fermi level (*12*, *14*, *19*). To this end, recently discovered 2D-vdW ferromagnetic monolayers (MLs) such as CrI_3 (*20*) appear to offer an optimal way to magnetize the TSSs of TIs. First, the Curie temperature of the CrI_3 ML is as high as 45 K (*20*), and it is hence conceivable that the T_c of the QAHE in CrI_3/TI heterostructures can be far higher than that in the Cr-doped $(Bi, Sb)_2Te_3$ thin films (*9*). Furthermore, the CrI_3 ML is a semiconductor, and thus, the transport properties of TIs should be preserved. Nevertheless, magnetic ions in most 2D-vdW magnetic materials such as Cr^{3+} ions in CrI_3 are typically covered by nonmagnetic layers in both sides; it is thus questionable whether their spin polarization can be sensed by TSSs, although the latter have a fairly large spatial extension.

Here, we report results of systematic computational studies based on the density functional theory (DFT) that suggest the possibility of using a CrI_3 ML to magnetize the TSSs of a prototypical 3D TI: Bi_2Se_3 (BS). We build up inversion-symmetric CrI_3/BS/CrI_3 heterostructures with a varying thickness for the BS films, from three to seven quintuple layers (QLs). We find that the TSSs of BS can be effectively magnetized by the CrI_3 ML in all cases. However, we show that CrI_3/BS/CrI_3 becomes a Chern insulator only when the BS film is thicker than five QLs. This results from the competition between the exchange field from CrI_3 and the remaining interaction between two surfaces of the BS film. This work reveals the subtleness of designing topological spintronic materials and provides a general guidance for the realization of the QAHE at high temperatures by combining 3D TIs with 2D-vdW magnetic MLs (*20*, *21*).

RESULTS

Electronic properties of CrI_3/BS/CrI_3 heterostructures

CrI_3 ML is a robust 2D semiconducting ferromagnet. It has a perpendicular magnetic anisotropy and a reasonably high Curie temperature (45 K) (*20*). Structurally, CrI_6 octahedrons form a honeycomb lattice. The optimized lattice constant of the pristine CrI_3 ML is a_{CrI3} = 7.04 Å, consistent with the previous theoretical result (*22*). This value is only 2.5% smaller than the size of the $\sqrt{3} \times \sqrt{3}$ BS supercell (7.22 Å), and hence, we stretch the CrI_3 ML so as to use a manageable unit cell for the simulation of CrI_3/BS/CrI_3. We find that all main properties of the CrI_3 ML are not substantially affected by the small lattice stretch (see fig. S1 and table S1).

There are three possible highly symmetric alignments between the $\sqrt{3} \times \sqrt{3}$ BS supercell and the CrI_3 ML, i.e., with Cr ions taking the Se, hollow, or Bi sites on BS (Fig. 1A), respectively. The calculated binding energies suggest that Cr^{3+} cations prefer to sit on the top of Se^{2-} anions (see fig. S2). The optimized interlayer distances between the CrI_3 ML and the BS surface are in a range from 3.07 to 3.12 Å, depending on the thickness of the BS film (see fig. S3). Note that the energy change is very small as we shift the CrI_3 ML in the lateral plan, so it is crucial to impose the inversion symmetry during the structural optimization. Here, we only discuss electronic and magnetic properties of the most stable configuration.

To shed some light on the interaction across the CrI_3/BS interface, we plot the charge density difference $\Delta\rho$ of CrI_3/BS/CrI_3, using six-QL BS as an example in Fig. 1B. The charge redistribution only occurs within a couple of atomic layers in BS, and the magnitude of $\Delta\rho$ is small. In particular, there is no observable net charge transfer between CrI_3 and BS. This is understandable since the bandgap of the freestanding CrI_3 ML is rather wide (larger than 1 eV). The interfacial Se atoms acquire a small but meaningful magnetic moment of −0.003 μ_B, which aligns antiparallelly with the magnetic moments of Cr^{3+} ions. The planar-averaged spin density $\Delta\sigma$ (Fig. 1C) shows that the negative spin polarization penetrates through the top half of the first QL of BS, following the direction of spin polarization of the iodine atoms.

[1]Department of Physics and Astronomy, University of California, Irvine, CA 92697-4575, USA. [2]Department of Physics, Incheon National University, Incheon 22012, Korea.
*Corresponding author. Email: wur@uci.edu

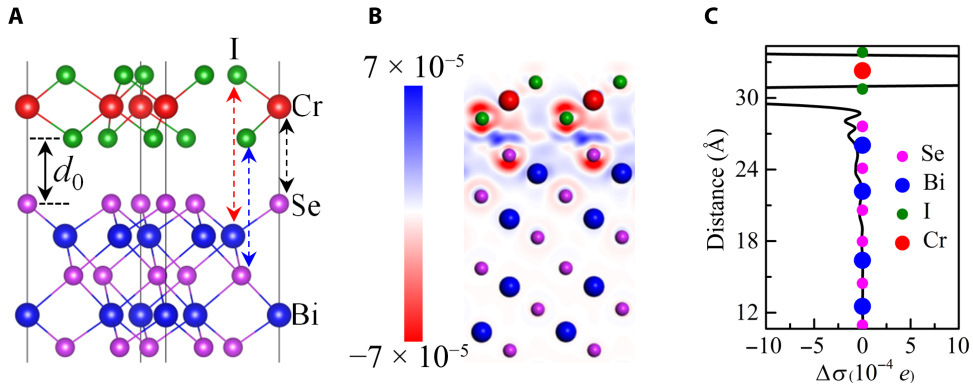

Fig. 1. Atomic structure and charge difference in CrI_3/BS/CrI_3. (**A**) Side view of the most stable CrI_3/BS/CrI_3. The green, red, pink, and blue balls are for I, Cr, Se, and Bi atoms, respectively. Dashed lines show the alignments between atoms in CrI_3 and BS layers; d_0 denotes the optimized vdW gap. (**B**) Real-space distribution of the charge difference $\Delta\rho = \rho_{total} - \rho_{BS} - \rho_{CrI_3}$ and (**C**) planar-averaged spin density $\Delta\sigma = \rho_\uparrow - \rho_\downarrow$ in the interfacial region of the CrI_3/6QL-BS/CrI_3 heterostructure.

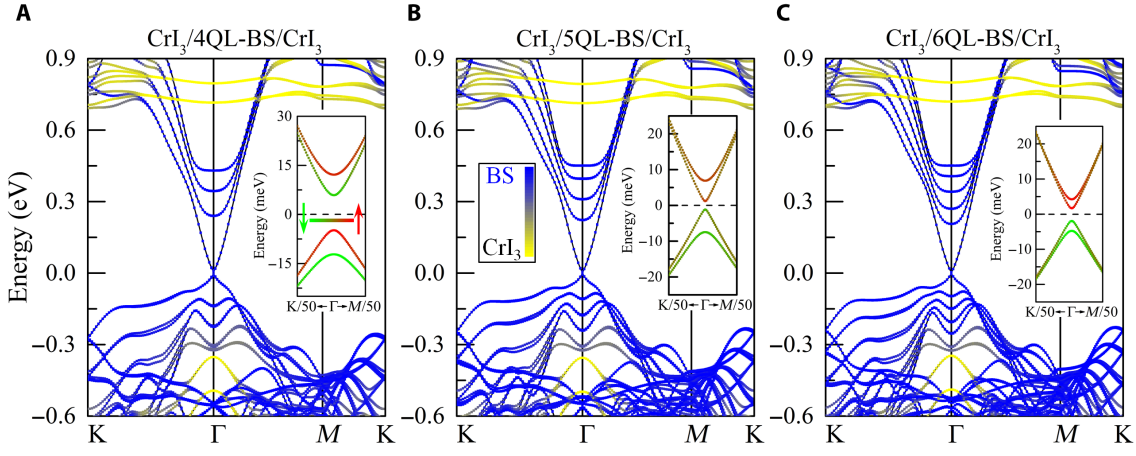

Fig. 2. Band structures of CrI_3/BS/CrI_3. DFT-calculated band structures of (**A**) CrI_3/4QL-BS/CrI_3, (**B**) CrI_3/5QL-BS/CrI_3, and (**C**) CrI_3/6QL-BS/CrI_3. Insets in (A), (B), and (C) are the fine band structures around the Fermi level. Colors in the main panels indicate the weights of bands from BS (blue) and CrI_3 (yellow). Colors in insets indicate the spin projections.

The calculated band structures of CrI_3/BS/CrI_3 with different thicknesses of BS (four, five, and six QLs) are shown in Fig. 2 (A to C, respectively). One important feature is that bands near the Fermi level are predominantly from BS, and CrI_3 states lie either 0.7 eV above the Fermi level or at least 0.3 eV below the Fermi level. As a result, the Dirac cone feature of TSSs are well maintained, or more explicitly, (i) all three cases have bandgaps of several millielectron volts at the Γ point and (ii) the spin degeneracies of TSSs are lifted, indicating that the TSSs of BS are magnetized by the CrI_3 ML. These results suggest the suitability of using vdW magnetic MLs to realize QAHE, instead of using conventional ferromagnetic or antiferromagnetic films that damage TSSs (*14*, *15*, *19*, *23*).

Topological properties of CrI_3/BS/CrI_3 heterostructures

To examine whether the magnetized TSSs of BS by CrI_3 MLs are topologically nontrivial, we take CrI_3/4QL-BS/CrI_3 and CrI_3/5QL-BS/CrI_3 as examples and calculate their Chern numbers C_N by integrating the Berry curvature in the first Brillouin zone with the Wannier90 package (see figs. S4 and S5). The Chern numbers of CrI_3/4QL-BS/CrI_3 and CrI_3/5QL-BS/CrI_3 are $C_N^{4QL} = 0$ and $C_N^{5QL} = 1$, respectively. This indicates that the former is a normal insulator but the latter is a Chern insulator. As shown in Fig. 3A, the QAHE state of CrI_3/5QL-BS/CrI_3 is further confirmed by the presence of one chiral edge state that connects the valance and conduction bands.

We use a low-energy effective four-band Hamiltonian to thoroughly study the topological properties of all CrI_3/BS/CrI_3 films. Note that states of CrI_3 MLs are far away from the Fermi level and that the effect of CrI_3 ML on TSSs of BS can be represented by an exchange field (H_{Zeeman}) and an interfacial potential ($H_{Interface}$). Hence, the low-energy effective four-band Hamiltonian (*2*, *5*, *6*) within the basis set of $\{|t,\uparrow\rangle, |t,\downarrow\rangle, |b,\uparrow\rangle, \text{and } |b,\downarrow\rangle\}$ is

$$H(k_x,k_y) = H_{surf}(k_x,k_y) + H_{Zeeman}(k_x,k_y) + H_{Interface}(k_x,k_y)$$
$$= A(k_x^2 + k_y^2) + \begin{bmatrix} 0 & iv_F k_- & M_k & 0 \\ -iv_F k_+ & 0 & 0 & M_k \\ M_k & 0 & 0 & -iv_F k_- \\ 0 & M_k & iv_F k_+ & 0 \end{bmatrix} +$$
$$\begin{bmatrix} \Delta & 0 & 0 & 0 \\ 0 & -\Delta & 0 & 0 \\ 0 & 0 & \Delta & 0 \\ 0 & 0 & 0 & -\Delta \end{bmatrix} + \begin{bmatrix} V_p & 0 & 0 & 0 \\ 0 & V_p & 0 & 0 \\ 0 & 0 & -V_p & 0 \\ 0 & 0 & 0 & -V_p \end{bmatrix} \quad (1)$$

Here, t and b denote the top and bottom surface states, respectively; ↑ and ↓ represent the spin up and down states, respectively; v_F and $k_\pm = k_x \pm ik_y$ are the Fermi velocity and wave vectors, respectively;

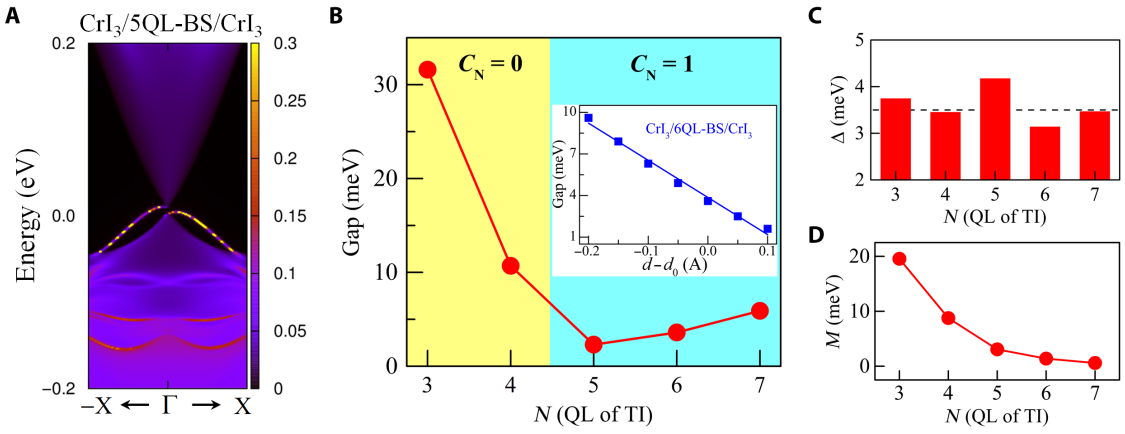

Fig. 3. Topological properties of CrI_3/BS/CrI_3. (**A**) Chiral edge state of the Chern insulator CrI_3/5QL-BS/CrI_3 ribbon. (**B**) Dependence of Chern numbers and gaps of CrI_3/BS/CrI_3 on the number (*N*) of QLs of BS. The inset shows the dependence of bandgaps of CrI_3/6QL-BS/CrI_3 on the CrI_3-BS interlayer distance *d*. d_0 is the optimized interfacial distance. (**C**) and (**D**) show the fitting parameters Δ and *M* in different CrI_3/BS/CrI_3 heterostructures, respectively. The horizontal dashed line in (B) shows the position of 3.5 meV.

and $M_k = M - B(k_x^2 + k_y^2)$ describes the coupling between the top and bottom TSSs. Note that *M* represents the gap produced by this coupling rather than magnetization as conventionally used, Δ is the exchange field from CrI_3, and V_p represents the magnitude of the asymmetric interfacial potential. Although V_p vanishes in the models with inversion symmetry, the situation in experiments can be changed by the misalignment of two CrI_3 MLs and by the presence of substrates and cover layers. Therefore, we keep the V_p term to hold the generality of our discussions. As shown in fig. S6 and table S2, the DFT bands of CrI_3/BS/CrI_3 around the Γ point can be fitted well by this Hamiltonian, indicating its applicability to these systems. The Berry curvature $\Omega(\boldsymbol{k})$ and Chern number C_N are calculated on the basis of the formulas in (*24*).

There is a clear phase boundary in Fig. 3B for the topological feature of CrI_3/BS/CrI_3, i.e., $C_N = 0$ ($C_N = 1$), when BS is thinner (thicker) than five QLs, consistent with the Chern numbers obtained by Wannier functions in CrI_3/BS/CrI_3 with four- and five-QL BS. Therefore, CrI_3/BS/CrI_3 heterostructures with less than five QLs of BS are normal insulators, and five QLs of BS are required to realize the QAHE in experiments. The calculated bandgaps of CrI_3/5QL-BS/CrI_3, CrI_3/6QL-BS/CrI_3, and CrI_3/7QL-BS/CrI_3 are 2.3 meV (27 K), 3.6 meV (42 K), and 5.9 meV (68 K), respectively. Equation 1 shows that its bandgap is $2|M - \Delta|$ (here, $M > 0$ and $\Delta > 0$). On the basis of the data in Fig. 3 (C and D), we see that the increase of bandgap with the BS thickness mainly results from the monotonic decrease of *M*. Moreover, the nontrivial bandgap of CrI_3/BS/CrI_3 noticeably increases with the reduction of *d* (see the inset in Fig. 3B for CrI_3/6QL-BS/CrI_3), indicating that it is beneficial to make *d* smaller through an external pressure for the realization of QAHE. Considering that the ML CrI_3 has a T_c of 45 K (*20*) and no other complex factors, such as uncontrollable distribution of dopants, local magnetic ordering, and charge transfer, are involved in these systems, we believe that QAHE should be observable in CrI_3/BS/CrI_3 heterostructures up to a few tens of kelvins, much higher than the temperature achieved with the doping approach (*9*–*11*).

In general, we find rules that govern topological properties of CrI_3/BS/CrI_3, i.e., (i) $C_N = 1$ when $\Delta^2 > M^2$ and (ii) $C_N = 0$ when $\Delta^2 < M^2$. This is consistent with the phase diagram in (*5*) and gives simple ways to manipulate the topological properties of systems with a 2D magnetic ML on TI. As shown in the Fig. 3C, the exchange field Δ slightly depends on the thickness of the BS film and fluctuates around 3.5 meV. This result is understandable since exchange field Δ mainly depends on the interfacial interaction between CrI_3 and BS. As expected, *M* has a strong dependence on the thickness of the BS film and exponentially decreases as the BS film becomes thicker (Fig. 3D). Note that the very small $M = 0.5$ meV in CrI_3/7QL-BS/CrI_3 is consistent with the experimentally observed gap closing in BS films thicker than six QLs (*25*). Since V_p is zero in CrI_3/BS/CrI_3 films with the inversion symmetry, the Hamiltonian equation 1 can be rewritten in terms of the basis of $\{|+,\uparrow\rangle, |-,\downarrow\rangle, |+,\downarrow\rangle$, and $|-,\uparrow\rangle\}$ with $|\pm,\uparrow\rangle = (|t,\uparrow\rangle \pm |b,\uparrow\rangle)/\sqrt{2}$ and $|\pm,\downarrow\rangle = (|t,\downarrow\rangle \pm |b,\downarrow\rangle)/\sqrt{2}$ as (*2*, *5*)

$$\tilde{H}(k_x, k_y) = A(k_x^2 + k_y^2) + \begin{bmatrix} H_+(k_x, k_y) & 0 \\ 0 & H_-(k_x, k_y) \end{bmatrix} \quad (2)$$

In Eq. 2, $H_\pm(k_x, k_y) = v_F k_y \sigma_x \mp v_F k_x \sigma_y + [M \pm \Delta - B(k_x^2 + k_y^2)]\sigma_z$ and $\sigma_{x,\,y,\,z}$ are Pauli matrices. From this Hamiltonian, we can get that the condition of $\Delta^2 > M^2$ leads to only one of the band inversions, either in $H_+(k_x, k_y)$ or in $H_-(k_x, k_y)$, and a Chern number $C_N = \Delta/|\Delta|$ (see table S3). This is understandable because the exchange splitting Δ can overcome the coupling-induced gap *M* in this condition and cause the band inversion of a pair of spin subbands (*26*). In CrI_3/BS/CrI_3 with four-QL or thinner BS, we have $\Delta^2 < M^2$ and hence $C_N = 0$. In contrast, thicker CrI_3/BS/CrI_3 films satisfy the condition of $\Delta^2 > M^2$ and hence become topologically nontrivial with $C_N = 1$. Even in the case that the top and bottom TSSs are completely decoupled, i.e., both $M = 0$ and $B = 0$, the exchange field Δ from the CrI_3 ML still leads to the QAHE in CrI_3/BS/CrI_3 as a result of the unique half-integer quantum Hall of the 2D massive Dirac Fermion in the two surfaces of the 3D TI (*5*, *6*, *27*).

To explore the effect of inversion symmetry breakdown, we investigate the evolution of band structure of CrI_3/6QL-BS/CrI_3 as the asymmetric interface potential V_p increases. The original topologically nontrivial bands (Fig. 4A) gradually change to M- and W-shaped bands (Fig. 4C) for $V_p > 2.8$ meV. Similar M- and W-shaped bands induced by V_p are also reported in a previous work (*28*). The bottom panel of Fig. 4D shows the Berry curvature of the occupied bands as $V_p = 5.0$ meV. One may see regions with both negative and positive Berry curvatures around the Γ point. This is different from the Berry

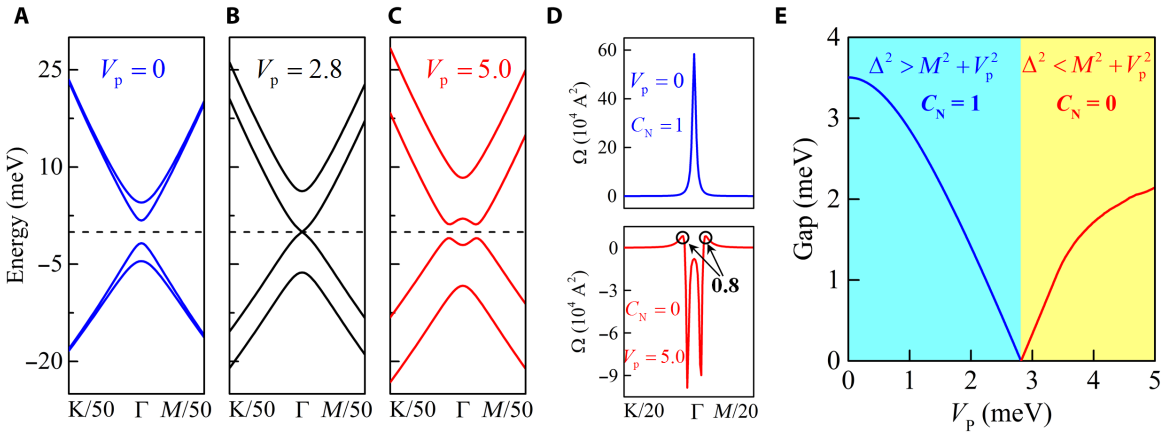

Fig. 4. Effect of V_p on the topological properties of CrI_3/6QL-BS/CrI_3. (**A**) to (**C**) show band evolutions with V_p increasing from 0 to 5.0 meV. (**D**) Berry curvatures of occupied bands around the Γ point for V_p = 0 (A, top) and V_p = 5.0 meV (C, bottom). The large positive Berry curvatures in the bottom panel are highlighted by black circles. (**E**) Dependence of Chern numbers and gaps on V_p Δ=3.1 meV and M = 1.4 meV are adopted in these calculations.

curvature for the $V_p = 0$ case shown in the top panel of Fig. 4D, where only a huge positive Berry curvature appears. With the presence of V_p, the criterion for the topological phase transition can be extended as follows (*5*): (i) When $\Delta^2 > M^2 + V_p^2$, $C_N = 1$, and (ii) when $\Delta^2 < M^2 + V_p^2$, $C_N = 0$. Note that it is counterintuitive that M- and W-shaped bands induced by the asymmetric interface potential V_p is topologically trivial. This shows the subtleness of identifying a topological state of CrI_3/BS/CrI_3 heterostructures or probably all analogous material systems. Note that the presence of V_p quickly reduces the topologically nontrivial gap in the Chern insulator region (Fig. 4E). This shows the importance of maintaining the inversion symmetry of CrI_3/BS/CrI_3 heterostructures for the realization of QAHE and other exotic quantum properties (*26*).

DISCUSSION

Magnetizing TSSs of TIs is of great importance as it gives rise to QAHE and many other novel phenomena, especially the hallmark of 3D TIs—the topological magnetoelectrical effect (*27*). We noted that large spin splitting might be produced in TSSs through δ codoping of Mn and Se(Te) in the topmost QL of TIs (*29*), but this may involve issues regarding the distribution and magnetic ordering of dopants. As magnetic insulators such as MnSe and EuS damage TSSs or shift TSSs away from the Fermi level (*12*, *14*, *19*), the emergent 2D-vdW magnetic MLs (*20*, *21*) offer unique opportunities to magnetize TSSs through the proximity effect as demonstrated in the present work.

In summary, using CrI_3/BS/CrI_3 heterostructures as modeling systems, we demonstrated that the emergent 2D-vdW magnetic MLs can effectively magnetize TSSs of TIs and also maintain their topological characteristics around the Fermi level. Furthermore, our analyses with an effective four-band Hamiltonian verify that CrI_3/BS/CrI_3 are Chern insulators when the BS film is five QLs or thicker. Their bandgaps are a few millielectron volts, and we believe that the QAHE is observable in these heterostructures at a temperature of a few tens of kelvins. As the family of 2D-vdW magnetic MLs steadily expands, it is foreseeable that even a higher-temperature QAHE can be achieved. According to discussions above, promising 2D-vdW magnetic MLs should have strong magnetization, large spatial extension of spin density, and shorter interfacial distance to TI surfaces.

MATERIALS AND METHODS

We used the Vienna Ab initio Simulation Package at the level of the generalized gradient approximation (*30*, *31*) in this work. The projector-augmented wave pseudopotentials were adopted to describe the core-valence interaction (*32*, *33*), and the energy cutoff for the plane-wave expansion was set to 500 eV (*31*). As shown in Fig. 1A, we constructed inversion-symmetric CrI_3/BS/CrI_3 slab models with a $\sqrt{3} \times \sqrt{3}$ BS supercell in the lateral plane to match the CrI_3 ML. The vacuum space between adjacent slabs was set to 15 Å. Atomic structures were fully optimized with a criterion that requires the force on each atom being less than 0.01 eV/Å. To correctly describe the weak interaction across CrI_3 and BS layers and the strong relativistic effect in Bi and I atoms, we included the nonlocal vdW functional (optB86b-vdW) (*34*) and the spin-orbit coupling (SOC) term in the self-consistent iterations. Furthermore, the local-spin-density approximations plus U (LSDA+U) method (*35*), with the on-site Coulomb interaction U = 3.0 eV and the exchange interaction J = 0.9 eV, was adopted to take the strong correlation effect of Cr 3*d* electrons into account. Topological properties of CrI_3/BS/CrI_3 slabs were studied by using effective Hamiltonians and the Wannier90 package (*36*). Test calculations indicate that the topological properties of CrI_3/BS/CrI_3 are very robust against the choices of U (fig. S7).

SUPPLEMENTARY MATERIALS

Supplementary material for this article is available at http://advances.sciencemag.org/cgi/content/full/5/5/eaaw1874/DC1

Table S1. Magnetic moment, bandgap, magnetocrystalline anisotropy energy, and Heisenberg exchange interactions J_1 and J_2.

Table S2. Parameters of the effective four-band model (see Eq. 1 in the main text) are used to fit the DFT-calculated band of CrI_3/BS/CrI_3.

Table S3. Analysis of band inversions and the Chern number C_N with respect to parameters Δ, M, and B.

Fig. S1. DFT + SOC + U–calculated band structure of the CrI_3 ML with pristine and stretched lattice constants.

Fig. S2. Top views of the three highly symmetric alignments between CrI_3 and BS in CrI_3/BS/CrI_3 heterostructures.

Fig. S3. Dependence of the binding energies and the vdW gaps of CrI_3/BS/CrI_3 on the number (N) of QL of BS.

Fig. S4. Topological properties of CrI_3/4QL-BS/CrI_3.

Fig. S5. Topological properties of CrI_3/5QL-BS/CrI_3.

Fig. S6. DFT-calculated (black lines) and fitted band structures (red dashed lines) of CrI_3/BS/CrI_3 based on the effective four-band model (see Eq. 1 in the main text).

Fig. S7. Effect of U on the topological properties of CrI_3/BS/CrI_3.

REFERENCES AND NOTES

1. M. Z. Hasan, C. L. Kane, Colloquium: Topological insulators. *Rev. Mod. Phys.* **82**, 3045–3067 (2010).
2. R. Yu, W. Zhang, H.-J. Zhang, S.-C. Zhang, X. Dai, Z. Fang, Quantized anomalous Hall effect in magnetic topological insulators. *Science* **329**, 61–64 (2010).
3. G. J. Ferreira, D. Loss, Magnetically defined qubits on 3D topological insulators. *Phys. Rev. Lett.* **111**, 106802 (2013).
4. H. Weng, R. Yu, X. Hu, X. Dai, Z. Fang, Quantum anomalous Hall effect and related topological electronic states. *Adv. Phys.* **64**, 227–282 (2015).
5. J. Wang, B. Lian, S.-C. Zhang, Quantum anomalous Hall effect in magnetic topological insulators. *Phys. Scr.* **2015**, 014003 (2015).
6. C.-X. Liu, S.-C. Zhang, X.-L. Qi, The quantum anomalous hall effect: Theory and experiment. *Annu. Rev. Condens. Matter Phys.* **7**, 301–321 (2016).
7. Y. L. Chen, J.-H. Chu, J. G. Analytis, Z. K. Liu, K. Igarashi, H.-H. Kuo, X. L. Qi, S. K. Mo, R. G. Moore, D. H. Lu, M. Hashimoto, T. Sasagawa, S. C. Zhang, I. R. Fisher, Z. Hussain, Z. X. Shen, Massive Dirac fermion on the surface of a magnetically doped topological insulator. *Science* **329**, 659–662 (2010).
8. L. A. Wray, S.-Y. Xu, Y. Xia, D. Hsieh, A. V. Fedorov, Y. S. Hor, R. J. Cava, A. Bansil, H. Lin, M. Z. Hasan, A topological insulator surface under strong Coulomb, magnetic and disorder perturbations. *Nat. Phys.* **7**, 32–37 (2011).
9. C.-Z. Chang, J. Zhang, X. Feng, J. Shen, Z. Zhang, M. Guo, K. Li, Y. Ou, P. Wei, L.-L. Wang, Z.-Q. Ji, Y. Feng, S. Ji, X. Chen, J. Jia, X. Dai, Z. Fang, S.-C. Zhang, K. He, Y. Wang, L. Lu, X.-C. Ma, Q.-K. Xue, Experimental observation of the quantum anomalous Hall effect in a magnetic topological insulator. *Science* **340**, 167–170 (2013).
10. C.-Z. Chang, W. Zhao, D. Y. Kim, H. Zhang, B. A. Assaf, D. Heiman, S.-C. Zhang, C. Liu, M. H. W. Chan, J. S. Moodera, High-precision realization of robust quantum anomalous Hall state in a hard ferromagnetic topological insulator. *Nat. Mater.* **14**, 473–477 (2015).
11. J. G. Checkelsky, R. Yoshimi, A. Tsukazaki, K. S. Takahashi, Y. Kozuka, J. Falson, M. Kawasaki, Y. Tokura, Trajectory of the anomalous Hall effect towards the quantized state in a ferromagnetic topological insulator. *Nat. Phys.* **10**, 731–736 (2014).
12. S. V. Eremeev, V. N. Men'shov, V. V. Tugushev, P. M. Echenique, E. V. Chulkov, Magnetic proximity effect at the three-dimensional topological insulator/magnetic insulator interface. *Phys. Rev. B* **88**, 144430 (2013).
13. P. Wei, F. Katmis, B. A. Assaf, H. Steinberg, P. Jarillo-Herrero, D. Heiman, J. S. Moodera, Exchange-coupling-induced symmetry breaking in topological insulators. *Phys. Rev. Lett.* **110**, 186807 (2013).
14. J. Kim, K.-W. Kim, H. Wang, J. Sinova, R. Wu, Understanding the giant enhancement of exchange interaction in Bi_2Se_3–EuS Heterostructures. *Phys. Rev. Lett.* **119**, 027201 (2017).
15. F. Katmis, V. Lauter, F. S. Nogueira, B. A. Assaf, M. E. Jamer, P. Wei, B. Satpati, J. W. Freeland, I. Eremin, D. Heiman, P. Jarillo-Herrero, J. S. Moodera, A high-temperature ferromagnetic topological insulating phase by proximity coupling. *Nature* **533**, 513–516 (2016).
16. C. Tang, C.-Z. Chang, G. Zhao, Y. Liu, Z. Jiang, C.-X. Liu, M. R. McCartney, D. J. Smith, T. Chen, J. S. Moodera, J. Shi, Above 400-K robust perpendicular ferromagnetic phase in a topological insulator. *Sci. Adv.* **3**, e1700307 (2017).
17. Z. Jiang, C.-Z. Chang, C. Tang, P. Wei, J. S. Moodera, J. Shi, Independent tuning of electronic properties and induced ferromagnetism in topological insulators with heterostructure approach. *Nano Lett.* **15**, 5835–5840 (2015).
18. X. Che, K. Murata, L. Pan, Q. L. He, G. Yu, Q. Shao, G. Yin, P. Deng, Y. Fan, B. Ma, X. Liang, B. Zhang, X. Han, L. Bi, Q.-H. Yang, H. Zhang, K. L. Wang, Proximity-induced magnetic order in a transferred topological insulator thin film on a magnetic insulator. *ACS Nano* **12**, 5042–5050 (2018).
19. W. Luo, X.-L. Qi, Massive Dirac surface states in topological insulator/magnetic insulator heterostructures. *Phys. Rev. B* **87**, 085431 (2013).
20. B. Huang, G. Clark, E. Navarro-Moratalla, D. R. Klein, R. Cheng, K. L. Seyler, D. Zhong, E. Schmidgall, M. A. McGuire, D. H. Cobden, W. Yao, D. Xiao, P. Jarillo-Herrero, X. Xu, Layer-dependent ferromagnetism in a van der Waals crystal down to the monolayer limit. *Nature* **546**, 270–273 (2017).
21. C. Gong, L. Li, Z. Li, H. Ji, A. Stern, Y. Xia, T. Cao, W. Bao, C. Wang, Y. Wang, Z. Q. Qiu, R. J. Cava, S. G. Louie, J. Xia, X. Zhang, Discovery of intrinsic ferromagnetism in two-dimensional van der Waals crystals. *Nature* **546**, 265–269 (2017).
22. J. Zhang, B. Zhao, T. Zhou, Y. Xue, C. Ma, Z. Yang, Strong magnetization and Chern insulators in compressedgraphene/CrI3van der Waals heterostructures. *Phys. Rev. B* **97**, 085401 (2018).
23. V. N. Men'shov, V. V. Tugushev, S. V. Eremeev, P. M. Echenique, E. V. Chulkov, Magnetic proximity effect in the three-dimensional topological insulator/ferromagnetic insulator heterostructure. *Phys. Rev. B* **88**, 224401 (2013).
24. Y. Yao, L. Kleinman, A. H. MacDonald, J. Sinova, T. Jungwirth, D.-s. Wang, E. Wang, Q. Niu, First principles calculation of anomalous hall conductivity in ferromagnetic bcc Fe. *Phys. Rev. Lett.* **92**, 037204 (2004).
25. Y. Zhang, K. He, C.-Z. Chang, C.-L. Song, L.-L. Wang, X. Chen, J.-F. Jia, Z. Fang, X. Dai, W.-Y. Shan, S.-Q. Shen, Q. Niu, X.-L. Qi, S.-C. Zhang, X.-C. Ma, Q.-K. Xue, Crossover of the three-dimensional topological insulator Bi_2Se_3 to the two-dimensional limit. *Nat. Phys.* **6**, 584–588 (2010).
26. X. Feng, Y. Feng, J. Wang, Y. Ou, Z. Hao, C. Liu, Z. Zhang, L. Zhang, C. Lin, J. Liao, Y. Li, L.-L. Wang, S.-H. Ji, X. Chen, X. Ma, S.-C. Zhang, Y. Wang, K. He, Q.-K. Xue, Thickness dependence of the quantum anomalous Hall effect in magnetic topological insulator films. *Adv. Mater.* **28**, 6386–6390 (2016).
27. X.-L. Qi, T. L. Hughes, S.-C. Zhang, Topological field theory of time-reversal invariant insulators. *Phys. Rev. B* **78**, 195424 (2008).
28. W.-Y. Shan, H.-Z. Lu, S.-Q. Shen, Effective continuous model for surface states and thin films of three-dimensional topological insulators. *New J. Phys.* **12**, 043048 (2010).
29. T. Hirahara, S. V. Eremeev, T. Shirasawa, Y. Okuyama, T. Kubo, R. Nakanishi, R. Akiyama, A. Takayama, T. Hajiri, S.-i. Ideta, M. Matsunami, K. Sumida, K. Miyamoto, Y. Takagi, K. Tanaka, T. Okuda, T. Yokoyama, S.-i. Kimura, S. Hasegawa, E. V. Chulkov, Large-gap magnetic topological heterostructure formed by subsurface incorporation of a ferromagnetic layer. *Nano Lett.* **17**, 3493–3500 (2017).
30. G. Kresse, J. Furthmüller, Efficient iterative schemes forab initiototal-energy calculations using a plane-wave basis set. *Phys. Rev. B* **54**, 11169–11186 (1996).
31. J. P. Perdew, K. Burke, M. Ernzerhof, Generalized gradient approximation made simple. *Phys. Rev. Lett.* **77**, 3865–3868 (1996).
32. P. E. Blochl, Projector augmented-wave method. *Phys. Rev. B* **50**, 17953–17979 (1994).
33. G. Kresse, D. Joubert, From ultrasoft pseudopotentials to the projector augmented-wave method. *Phys. Rev. B* **59**, 1758–1775 (1999).
34. J. Klimes, D. R. Bowler, A. Michaelides, Chemical accuracy for the van der Waals density functional. *J. Phys. Condens. Matter* **22**, 022201 (2010).
35. A. I. Liechtenstein, V. I. Anisimov, J. Zaanen, Density-functional theory and strong interactions: Orbital ordering in Mott-Hubbard insulators. *Phys. Rev. B* **52**, R5467–R5470 (1995).
36. A. A. Mostofi, J. R. Yates, Y.-S. Lee, I. Souza, D. Vanderbilt, N. Marzari, Wannier90: A tool for obtaining maximally-localised Wannier functions. *Comput. Phys. Commun.* **178**, 685–699 (2008).

Acknowledgments: DFT calculations were performed on parallel computers at NERSC. **Funding:** Work was supported by DOE-BES (grant no. DE-FG02-05ER46237). **Author contributions:** R.W. conceived the idea of this study. Y.H. performed DFT calculations. J.K. calculated the edge states. Y.H. and R.W. wrote the manuscript. All authors commented on the manuscript. **Competing interests:** The authors declare that they have no competing interests. **Data and materials availability:** All data needed to evaluate the conclusions in the paper are present in the paper and/or the Supplementary Materials. Additional data related to this paper may be requested from the authors.

Submitted 27 November 2018
Accepted 23 April 2019
Published 31 May 2019
10.1126/sciadv.aaw1874

Citation: Y. Hou, J. Kim, R. Wu, Magnetizing topological surface states of Bi_2Se_3 with a CrI_3 monolayer. *Sci. Adv.* **5**, eaaw1874 (2019).